MID-AMERICA TRANSPORTATION CENTER

Report # MATC-UI: 142-5

Final Report

WBS: 25-1121-0005-142-5

Infrastructure Inspection During and After Unexpected Events - Phase V

Salam Rahmatalla, PhD
Professor
Department of Civil and Environmental Engineering
University of Iowa

Casey Harwood, PhD
Assistant Professor
Department of Mechanical Engineering

Ali Karimpour, PhD
Postdoctoral Research Scholar
Department of Civil and Environmental Engineering

2023

A Cooperative Research Project sponsored by
U.S. Department of Transportation- Office of the Assistant Secretary for Research and Technology

The contents of this report reflect the views of the authors, who are responsible for the facts and the accuracy of the information presented herein. This document is disseminated in the interest of information exchange. The report is funded, partially or entirely, by a grant from the U.S. Department of Transportation's University Transportation Centers Program. However, the U.S. Government assumes no liability for the contents or use thereof.

Infrastructure Inspection During and After Unexpected Events – Phase V

Salam Rahmatalla, Ph.D.
Professor
Civil and Environmental Engineering
University of Iowa

Ali Karimpour, Ph.D.
Postdoctoral Research Scholar
Civil and Environmental Engineering
University of Iowa

Casey Harwood, Ph.D.
Assistant Professor
Mechanical Engineering
University of Iowa

A Report on Research Sponsored by

Mid-America Transportation Center

University of Nebraska-Lincoln

December 2022

Technical Report Documentation Page

1. Report No. 25-1121-0005-142-5	2. Government Accession No.	3. Recipient's Catalog No.
4. Title and Subtitle Infrastructure Inspection during and after Unexpected Events – Phase V		5. Report Date December 2022
		6. Performing Organization Code
7. Author(s) Salam Rahmatalla, Ali Karimpour, Casey Harwood		8. Performing Organization Report No. 25-1121-0005-142-5
9. Performing Organization Name and Address University of Iowa, College of Engineering 3100 Seamans Center for the Engineering Arts and Sciences Iowa City, IA 52242		10. Work Unit No. (TRAIS)
		11. Contract or Grant No. 69A3551747107
12. Sponsoring Agency Name and Address Mid-America Transportation Center 2200 Vine St. PO Box 830851 Lincoln, NE 68583-0851		13. Type of Report and Period Covered January 2021 – December 2021
		14. Sponsoring Agency Code MATC TRB RiP# 91994-98
15. Supplementary Note		

The effect of hydrodynamic added mass on bridge structures during flooding has been investigated in this work, and its secondary effects on the model dynamic characteristics and natural frequency were studied and developed in both experimental and numerical setup. The theoretical background of the added mass calculations plus numerical simulations have been conducted on both full-scale and small-scale models, while experimental studies have been conducted on only a small-scale model in a tilting flume at the University of Iowa hydraulic lab. After publishing a methodology to calculate added mass of inundated bridges in a journal, this work focused on the effects of the inundation depth with the flow current velocity on the hydraulic added mass quantity. Some preliminary experiments have been conducted, and both numerical and experimental tools and setups have been prepared and developed to perform parametric studies to capture the variability of the hydraulic added mass.

17. Key Words Structural Failure Mode, Finite Element Model (FEM), Highway Bridges, Integral Abutment System.		18. Distribution Statement	
19. Security Class if. (Of this report) Unclassified	20. Security Class if. (Of this page) Unclassified	21. No. of Pages 16	22. Price

Table of Contents

List of Figures

Disclaimer

The contents of this report reflect the views of the authors, who are responsible for the facts and the accuracy of the information presented herein. This document is disseminated under the sponsorship of the U.S. Department of Transportation's University Transportation Centers Program, in the interest of information exchange. The U.S. Government assumes no liability for the contents or use thereof.

Executive Summary

This report investigates the added mass effects of highway bridges which are prone to inundation during flood season or, hurricane events for coastal bridges. To quantify such parameters, it is necessary to exploit a strong theoretical formulation, numerical software, and experimental analysis to simulate such sophisticated events. Numerical modeling is required to simulate any extreme incidents in advance to capture structure performance, internal and external capacity, and demand for potential resolutions. The ultimate goal of this ongoing research is to identify conditions under which current AASHTO codes may be unconservative and to augment those formulas to account for inundation effects upon the resonances and bearing reaction forces of notional bridges.

Chapter 1 Introduction and Background

AASHTO's *Guide Specifications for Bridges Vulnerable to Coastal Storms* (AASHTO 2008) contains guidelines for estimating external forces and moments on bridge structures due to potential floods or storms. For the code in these guidelines, the external forces and moments are initially estimated with the assumption that the bridge is a rigid body and the resulting forces are imposed upon a structural model. This approach may underestimate the mutual interactions between the fluid forces and structural motions, which arise from fluid pressures and shear stresses. It is well-known that the fluid loading exerted in opposition to structural accelerations, termed *hydrodynamic added mass* (HAM), can cause tremendous changes in structural properties and responses during flooding and storms (Karimpour et al. 2022).

AASHTO's guide specification is the popular, widely applicable design code for estimating potential forces from fluids toward fluvial bridges during extreme hydro events. It is not clear if the proposed AASHTO loads may underestimate some of the forces, and dynamic effects may not be comprehensively considered. In a previous study (Karimpour et al. 2022), the authors proposed a methodology for calculating the directional HAM, which for a few representative bridges was demonstrated to be several times larger than the modal mass of the bridge structure itself.

Chapter 2 Hydrodynamic Added Mass during Floodings

To calculate the HAM of any model, the first step is to establish the coupled governing equations for the mediums of both fluid and structure. The discrete finite element (FE) formulation of the coupled acoustic structural (CAS) model can be expressed as follows (Rawat et al. 2019; Eslaminejad et al. 2019):

$$\begin{bmatrix} [\boldsymbol{M}_S] & \boldsymbol{0} \\ \rho_f [\boldsymbol{R}]^T & [\boldsymbol{M}_f] \end{bmatrix} \begin{Bmatrix} \ddot{\boldsymbol{u}} \\ \ddot{\boldsymbol{p}} \end{Bmatrix} + \begin{bmatrix} [\boldsymbol{C}_S] & \boldsymbol{0} \\ \boldsymbol{0} & [\boldsymbol{C}_f] \end{bmatrix} \begin{Bmatrix} \dot{\boldsymbol{u}} \\ \dot{\boldsymbol{p}} \end{Bmatrix} + \begin{bmatrix} [\boldsymbol{K}_S] & -[\boldsymbol{R}]^T \\ \boldsymbol{0} & [\boldsymbol{K}_f] \end{bmatrix} \begin{Bmatrix} \boldsymbol{u} \\ \boldsymbol{p} \end{Bmatrix} = \begin{Bmatrix} \boldsymbol{0} \\ \boldsymbol{0} \end{Bmatrix} \tag{2.1}$$

In the case of free vibration, equation (2.1 can be rewritten as follows:

$$\left(-\omega_n^2 \begin{bmatrix} [\boldsymbol{M}_S] & \boldsymbol{0} \\ \rho_f [\boldsymbol{R}]^T & [\boldsymbol{M}_f] \end{bmatrix} + j\omega_n \begin{bmatrix} [\boldsymbol{C}_S] & \boldsymbol{0} \\ \boldsymbol{0} & [\boldsymbol{C}_f] \end{bmatrix} + \begin{bmatrix} [\boldsymbol{K}_S] & -[\boldsymbol{R}]^T \\ \boldsymbol{0} & [\boldsymbol{K}_f] \end{bmatrix} \right) \begin{Bmatrix} \boldsymbol{u} \\ \boldsymbol{p} \end{Bmatrix} = \begin{Bmatrix} \boldsymbol{0} \\ \boldsymbol{0} \end{Bmatrix} \tag{2.2}$$

where $\boldsymbol{u}$, $\boldsymbol{p}$, $\boldsymbol{M}$, $\boldsymbol{C}$, $\boldsymbol{K}$, and $\boldsymbol{R}$ are the displacement degree of freedom (DOF) vector, the fluid acoustic pressure DOF, the mass, damping, and stiffness matrices, and the reaction impedance, respectively. In all cases, the subscript S indicates a structural quantity and the subscript f indicates a fluid quantity. The displacement vector $\boldsymbol{u}$ includes both structural and fluid displacements. The coupling between the two mediums is enforced by maintaining equal normal displacement/velocity (kinematic coupling) and equal normal stresses (dynamic coupling) at the interface between the solid and fluid domains. Matrix $\boldsymbol{R}$ is critical to the coupling of the fluid and structure by enforcing the compatibility of pressure and displacement at the interface.

Abaqus® software (SIMULIA 2021) was used in this work to simulate the coupling problem between the bridge structure and the surrounding fluid medium. A representative bridge model, shown in Figure 2.1, was chosen for further studies alongside a small-scale representative model (testbed). The numerical model is shown in Figure 2.2. The HAM of the small-scale model was quantified in both experimental and numerical analyses. To better understand HAM quantity importance and its effect on system dynamic characteristics, the numerical model was used to estimate the HAM of the full-scale bridge.

Figure 2.1 Representative bridge prototype and small-scale testbed used in the research.

The developed methodology indicated that the real prototype bridge can gain HAM up to 5.8 times its structural mass if it is excited around its first natural frequency in the inundation stage. To the authors' knowledge, no previous studies have investigated the large amount of HAM that occurs during the inundation stage when a turbulent source causes the system to vibrate to the first natural frequency and changes the medium from air to water. While AASHTO implicitly inserted a high safety factor in its quasi-static load formulas, it is not clear whether or how such dynamic HAM has been incorporated into the formulas, even though this could impose devastating external action into the system and cause bridge collapse. The complete research milestone and methodology is available in the reference Karimpour et al. (2022).

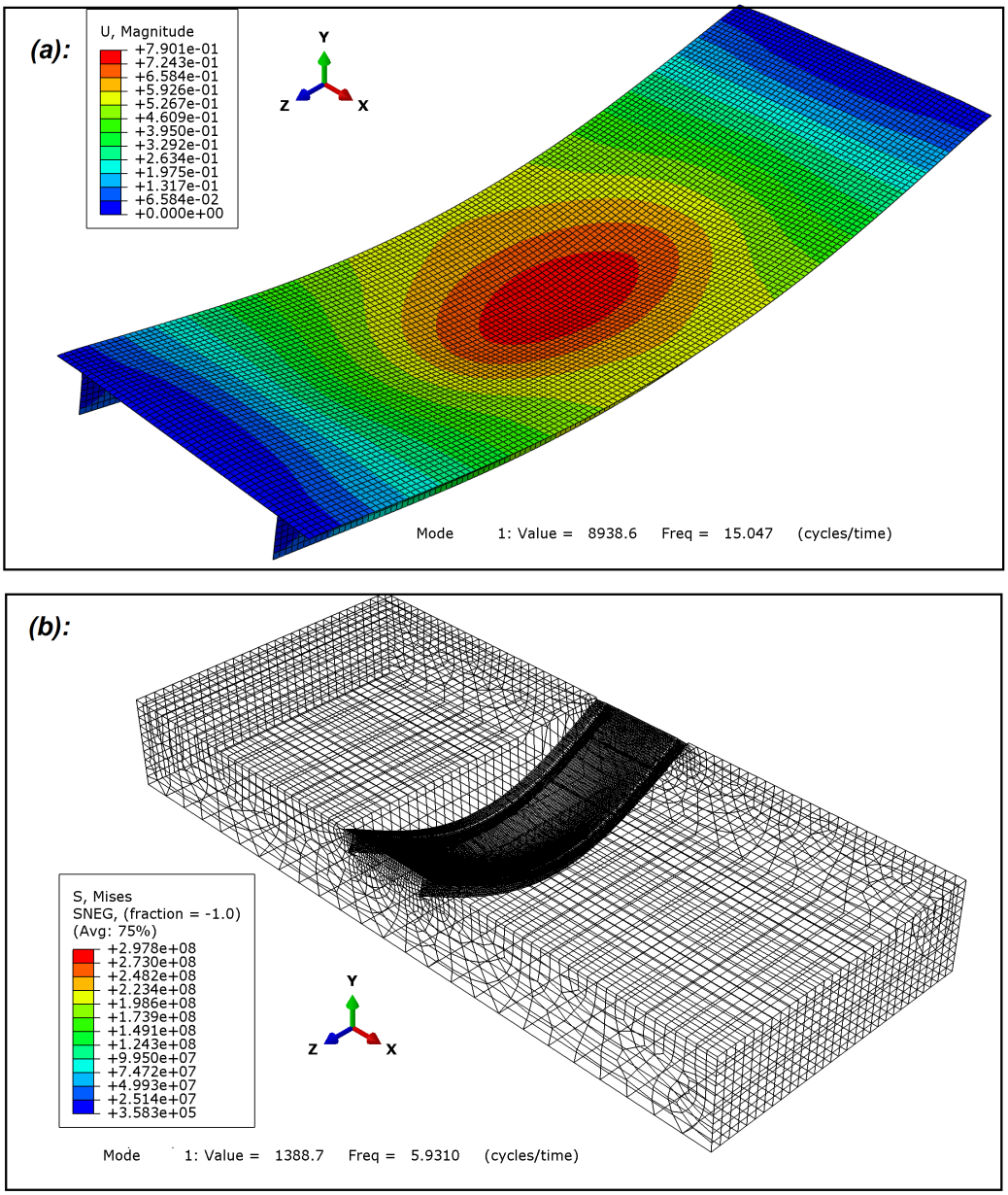

Figure 2.2 Numerical model of testbed: (a) first dynamic mode in dry condition; (b) first dynamic mode in wet condition.

Chapter 3 Testbed Experimental Setup with Shaker Excitation

The small-scale model (testbed) was excited by an electrodynamic shaker in both dry and wet conditions to determine the dry and wet natural frequencies, as shown in Figure 3.1. An electromagnetic shaker motor was used to produce an input force, which was transmitted through a drive-point impedance head to measure drive point force and acceleration. Four calibrated vertical load cells were placed to support the weight of the bridge model, with one at each corner of the bridge. The model itself was designed with pinned boundary conditions, achieved using hinges at each end of the span. Excitation signals were stored as audio WAV files and played back using a LabVIEW interface through a NI-9263 voltage output module with a sample rate of 44.1 kHz and 16-bit resolution. The drive point force and acceleration signals were acquired using an IEPE signal conditioner and digitizer module (NI-9230) at a sampling rate of 5 kHz and a resolution of 24 bits. The four corner-mounted load cells were acquired using a combination bridge-amplifier and digitizer unit (NI-9327) at a sampling rate of 5 kHz and 24-bit resolution. All input and output modules were hosted in a cDAQ-9188 chassis.

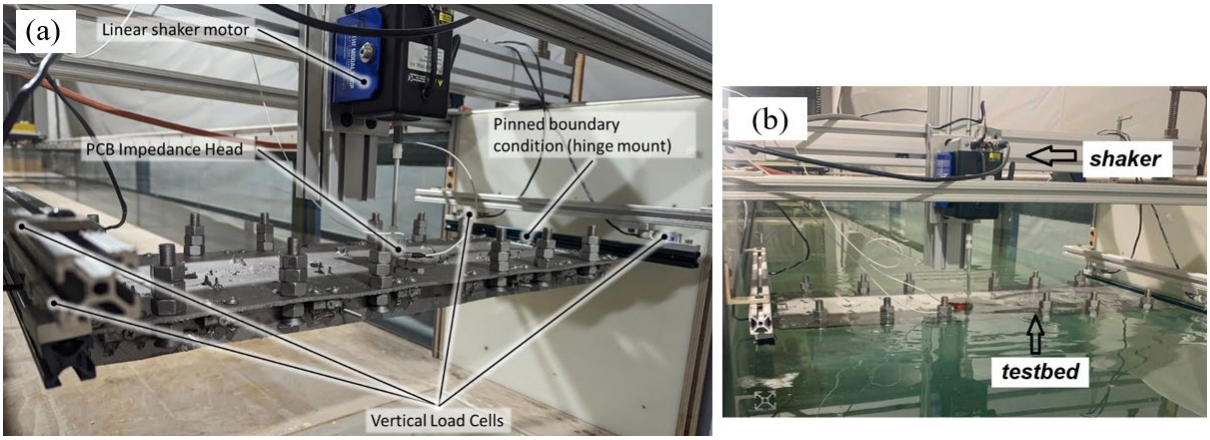

Figure 3.1 (a) The small-scale experimental setup with the shaker motor. (b) The inundated testbed mounted in the flume.

Excitation was performed using a quasi-random signal composed of a multitude of sinusoids at discrete frequencies. The shaker was fed with sine sweep and pseudo random signals up to 300 Hz in order to excite it with a low-band frequency range that would be similar to when bridges experience vibration in real flooding or hurricane events. Figure 3.2 plots the frequency response functions (FRFs) of the testbed based on the MATLAB® H1 estimator ('modalfrf' function), evaluated from the four output force signals, and the measured input driving acceleration signal.

Figure 3.3 shows the natural frequency extraction plot in the dry condition, while Figure 3.4 shows the same plot for a fully inundated condition. These plots show that all the detected natural frequencies dropped as a result of HAM when the bridge deck was submerged. In mode 1 it dropped from 12 Hz to 5.5 Hz, which was in close agreement with the numerical model previously simulated by the authors. The small discrepancy between models is related to the experimental setup, which is not the same as that simulated numerically. This huge variation in first mode natural frequency indicates a large amount of HAM when the model is excited around its first frequency during a flooding event.

More importantly, it demonstrates that varying immersion results in natural frequencies that vary significantly, producing wide bands of the frequency axis in which excitation may cause resonance at some immersion depth. If predictions of bridge natural frequencies are made without the inclusion of HAM, there exists a risk that unanticipated resonances may arise. This is especially true when ambient excitation—such as that due to fluvial flows—impinges on the bridge structure.

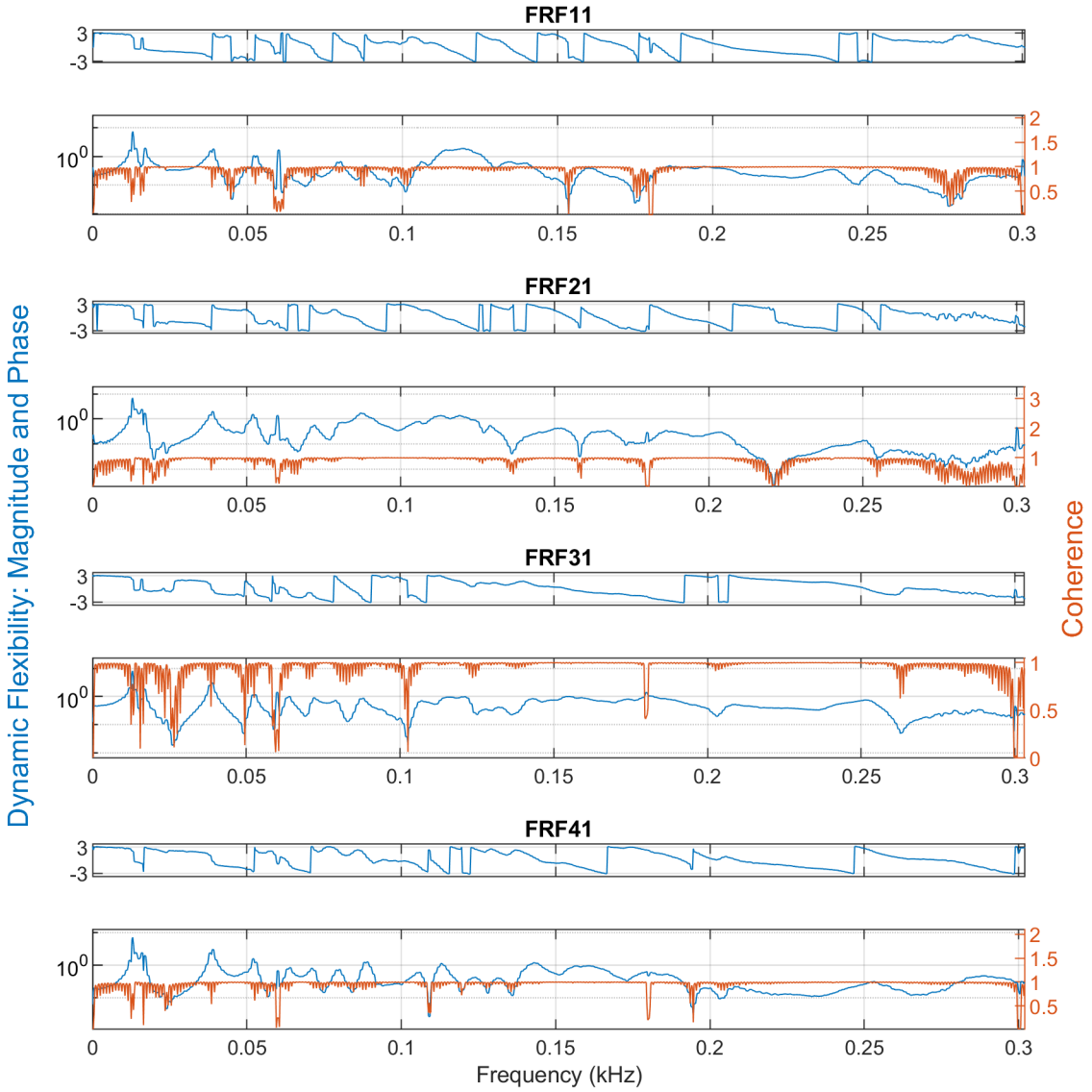

Figure 3.2 Testbed FRFs estimated from an input driving point force and four force signals excited by an electrodynamic shaker.

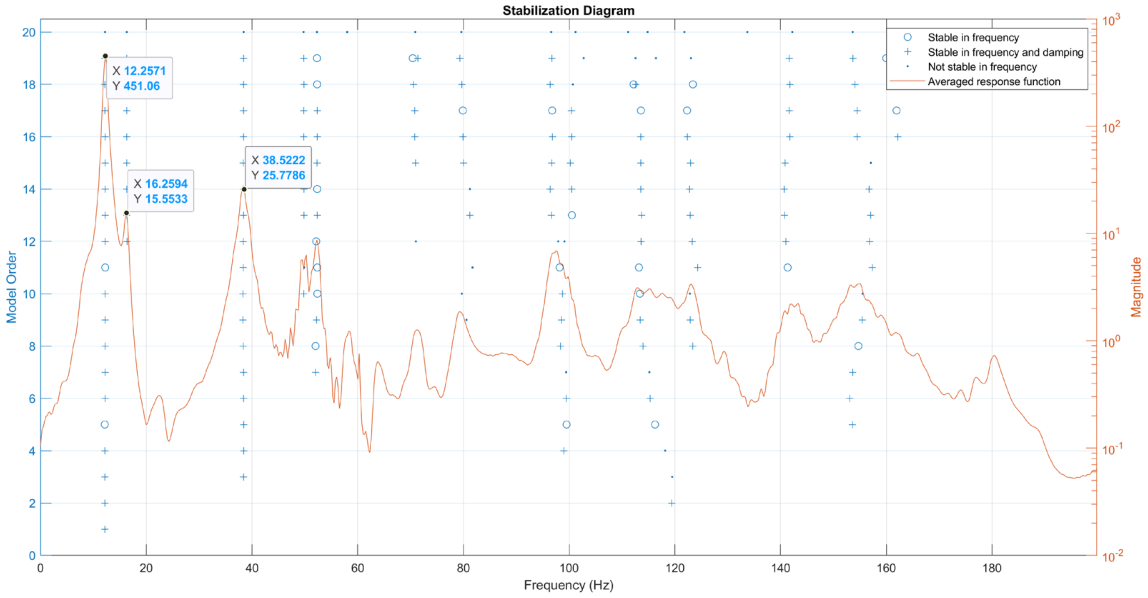

Figure 3.3 Stabilization plot to extract the natural frequency of the testbed in the dry condition.

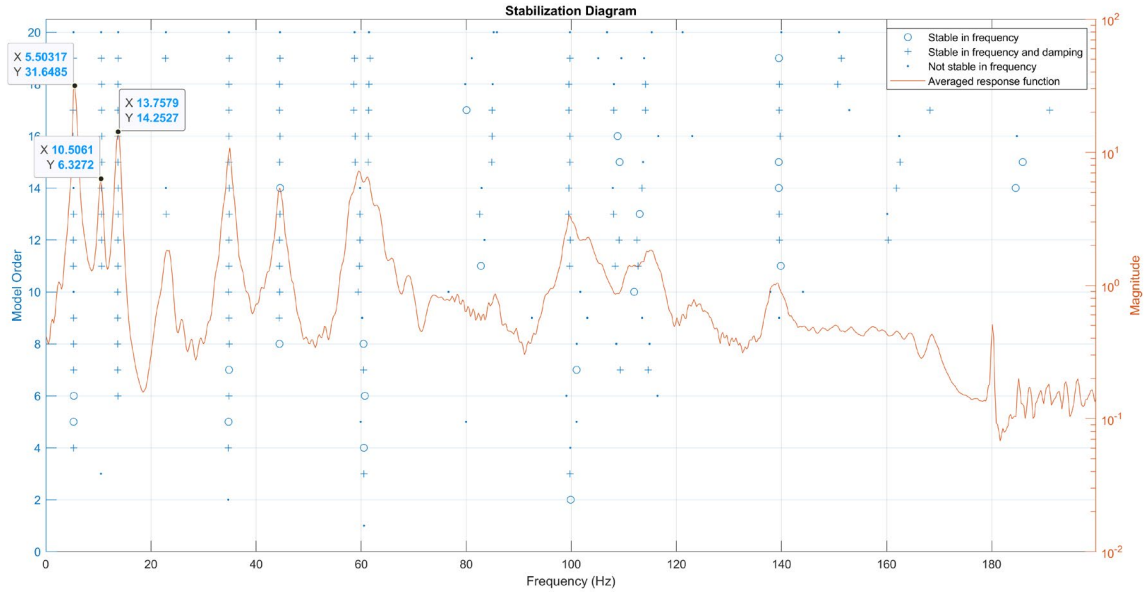

Figure 3.4 Stabilization plot to extract the natural frequency of the testbed in the wet condition.

Chapter 4 Effects of Inundation Depth and Current Speed on Hydrodynamic Added Mass

Previous studies (ASCE 2017) indicated that vibratory behavior (dynamic response) of the testbed could vary intensely as inundation depth and incoming current flow speed change during simulated flooding. Therefore, several experiments were conducted to investigate the inundation depth effect on the natural frequency variation of the system as shown in Figure 4.1. The experiments were executed with different flow depths by adjusting both the flume tailgate and the elevation of the flume's headbox (the latter adjusted by tilting the entire flume) to reach the desired water depth and flow speed at the bridge testbed. The hydrodynamic loading on the bridge was measured in the vertical direction, using four shear beam load cells at the corners of the testbed, which are anchored to the supporting structure of the flume.

Figure 4.1 Small-scale bridge testbed during a running flow experiment to see inundation depth effect.

The natural frequency has an inverse relationship with HAM: as it lowers, HAM increases. Figure 4.2 plots time series data from the four mounted force sensors that recorded when the flume tilt engine and flume water pump reached the steady-state condition. When looking at the time series, it is evident that the testbed at 10 inches overhead is almost stable, only experiencing hydrostatic pressure under and over its deck surface. As the overhead depth decreases, the oscillatory behavior can be captured from the sensors; while the model is under less hydrostatic pressure at a higher flow velocity, it prompts the model to vibrate more intensely than it does with a deeper overhead, especially around the model's first wet natural frequency. Figure 4.3 shows the spectrum of overlaid force sensor signals as overhead depth decreases from 10 inches to 1 inch. As evident in the plot, the energy under the spectrum is magnified as the overhead decreases from 10 inches to 3 inches and then attenuates again from 3 inches to 1 inch overhead. This means that at a 3-inch overhead depth, the model experiences intense vibration excitation with probable resonance at its natural frequency. Therefore, it can be concluded that such structures do not behave linearly as they enter the inundation stage, and a critical depth exists where the model energy input goes up uncontrollably at a much lower overhead inundation rather than at a greater depth, as shown here.

In these experiments, only overhead depth was changed to investigate the model frequency and vibration energy level variation; the flume pump was set at its maximum capacity to produce the maximum possible discharge. The current frequency must be incorporated into the investigation in future studies to better capture any of its realistic behavior. AASHTO (2008) provides only the simplest one-dimensional formula to estimate the streamway current load (horizontal component) towards the bridge superstructure, regardless of overtopped depth, and the formula is only a function of current velocity. The following is the AASHTO formula:

$$F_{HC} = C_d A \left(\frac{\rho_w}{2}\right) \frac{U_c^2}{1000} \tag{4.1}$$

where $C_d$is a suggested drag coefficient of 2.5, A is superstructure projected area per unit length of superstructure, ρ_w is unit mass of water taken as $1000(kg/m^3)$, and U_c is the current velocity (m/sec). For the testbed testing:

$$F_{HC} = 2.5\left(0.73 * \frac{0.05}{2}\right)\left(\frac{1000}{2}\right)(1^2) = \ 22.8N \tag{4.2}$$

As shown in Fig. (4.2), the vertical forces due to the current loadings can reach up to 8.7 times the horizontal force AASHTO predicts with its formula, but this vertical loading has not been introduced in the code. These high magnitude dynamic forces, generated due to the current only, could make the inundated bridge model experience damage. Considering the laws of similarity, the force quantity is scaled down by a power of three of the length scale, $\lambda_F = \lambda_L^3$, and the model scale of 1:60. The real bridge-imposed loads can be estimated by multiplying $\lambda_F = 60^3 = 216000$ by the small-scale model forces estimated here.

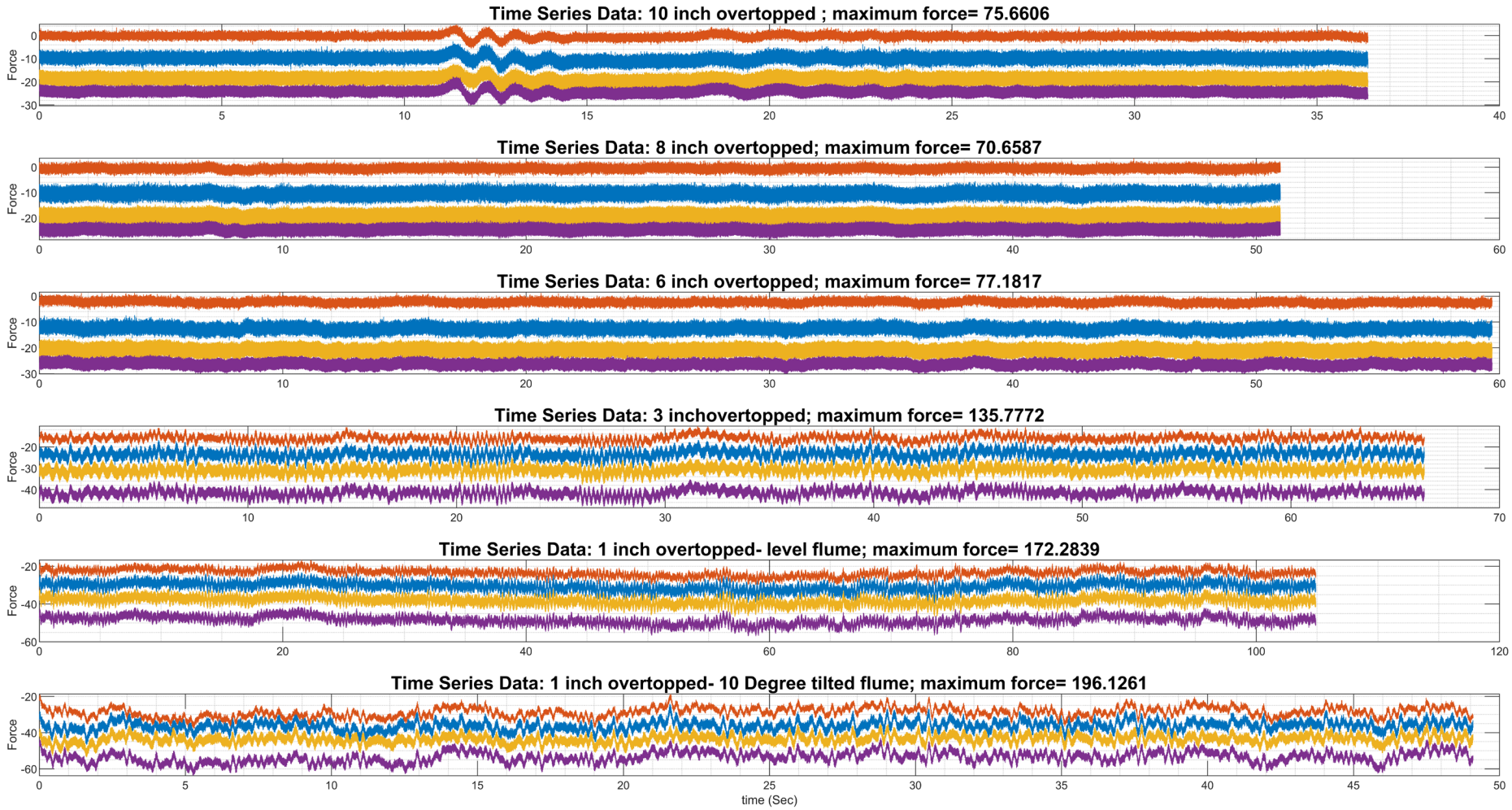

Figure 4.2 Time series of the testbed vertical force sensors data during experiments: (a) 10” overhead; (b) 8” overhead; (c) 6” overhead; (d) 3” overhead; (e) 1” overhead; (f) 1” overhead tilted flume.

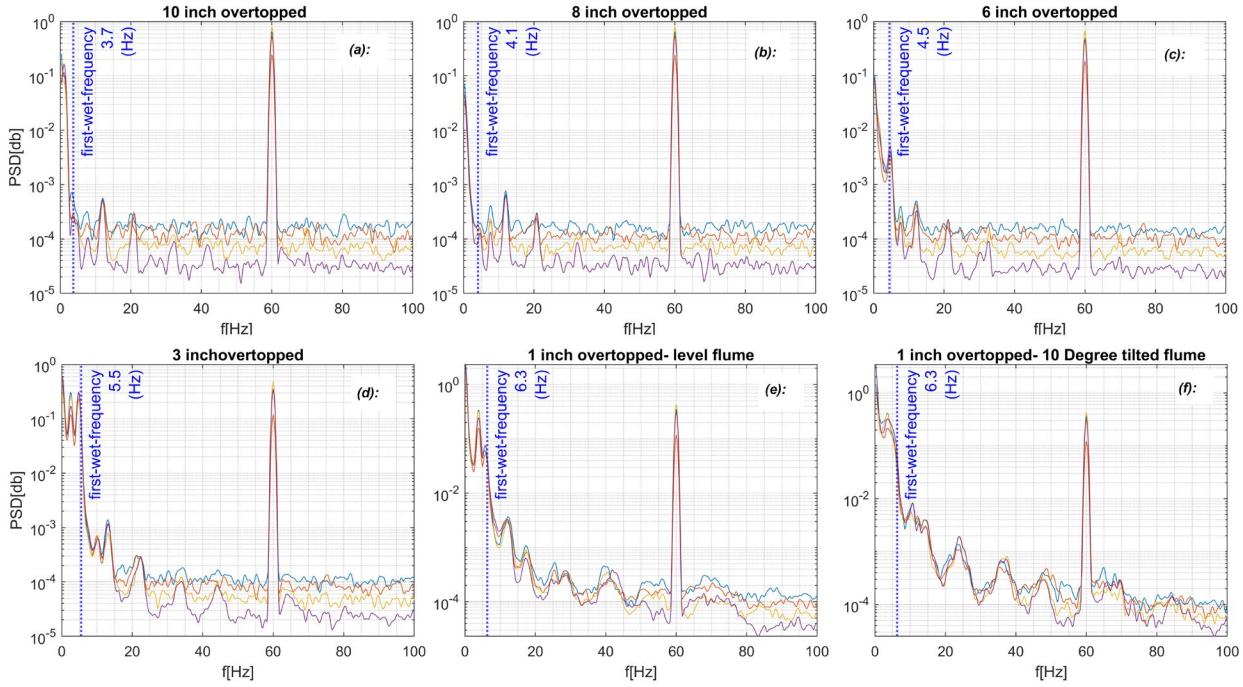

Figure 4.3 Spectrum plot of the testbed force sensors data during experiments: (a) 10” overhead; (b) 8” overhead; (c) 6” overhead; (d) 3” overhead; (e) 1” overhead; (f) 1” overhead, tilted flume.

Chapter 5 Conclusion

The hydrodynamic added mass calculation of inundated bridges during flooding/storm events has been developed, and a methodology based on natural frequency changes has been proposed and published in a journal paper. It was found that such quantity can be several times the bridge's overall mass in certain vibrational conditions and that AASHTO code does not indicate such an effect explicitly. The imposed forces could be larger than the proposed AASHTO formulas, especially for inundated bridges where the hydrodynamic added mass makes them much more vulnerable to low-frequency excitations. Thus, a small-scale testbed constructed from a representative bridge was used for experimental purposes, and recent experiments indicate that simulated flooding events can easily excite the first wet natural frequency of the structure, and that consequently a large hydrodynamic added mass can be incorporated into the system. It was also found that there is a critical condition of the current velocity and different overtopped depths, as an independent input could generate multiple magnitudes of the force to the system, as shown in Figure 4.2; however, much higher overtop heights would not impose much of an amount. Therefore, the future goals of the research will focus on two independent parameters (current velocity and inundation depth) of the added mass quantity, and then derive a parametric formula that relates those two independent parameters with the added mass. Both the flow current velocity and the flow overhead depth above the testbed can change the added mass quantity independently. To understand such a relationship in depth, both experimental and numerical simulations are needed to capture such incidental effects and could potentially be appended to the AASHTO formulas in the future.

References

AASHTO (2008). Guide specifications for bridges vulnerable to coastal storms, 1st Ed., AASHTO, Washington, DC.

Karimpour, A., Rahmatalla, S. and Harwood, C. (2022). Effect of directional added mass on highway bridge response during flood events. Infrastructures, 7(3), p.42.

Rawat, A., Matsagar, V.A., and Nagpal, A.K. (2019). Numerical study of base-isolated cylindrical liquid storage tanks using coupled acoustic-structural approach. Soil Dyn. Earthq. Eng., 119, 196–219.

Eslaminejad, A., Ziejewski, M., and Karami, G. (2019). An experimental–numerical modal analysis for the study of shell-fluid interactions in a clamped hemispherical shell. Appl. Acoust., 152, 110–117.

ASCE (2017). Minimum design loads and associated criteria for buildings and other structures. American Society of Civil Engineers.

SIMULIA (2021). Abaqus/Standard. SIMULIA - Dassault Systèmes, Providence, RI.

Yim, S.C., and Azadbakht, M., 2013. Tsunami forces on selected California coastal bridges. Technical Rep., Caltrans, Sacramento, CA.